Proceedings of the Institute of Acoustics

DISTORTION IMMUNITY OF MLS-DERIVED IMPULSE RESPONSE MEASUREMENTS

Chris Dunn (1) and Dr Malcolm Hawksford (2)

(1) and (2) University of Essex, Audio Research Group, Department of Electronic Systems Engineering, Wivenhoe Park, Colchester CO4 3SQ, U.K.

ABSTRACT

Maximum length sequences (MLS) are becoming widely used as an accurate method of determining the impulse response of audio transducers. Although MLS techniques offer an enhanced immunity to noise and distortion compared to periodic impulse testing, non-linearity in the measurement chain still results in impulse response errors. This paper examines the nature of such errors within typical measurement environments.

0 INTRODUCTION

Historically the determination of the linear transfer function has been the most fundamental evaluation of an audio system, defined by the impulse response (IR) in the time domain from which the frequency response can be calculated. The design of modern audio equipment requires ever more accurate methods of determining the linear transfer function. An example that illustrates such a need is equalisation of loudspeakers in the digital domain; digital signal processing allows equalised on-axis frequency response deviations of better than +/- 0.5 dB across wide regions of the audio spectrum [1]. Such high performance requires a similarly accurate measurement technique to ensure that the equalisation performed is the correct one; it is important to eradicate measurement artifacts at the beginning of the design cycle since errors can form a closed system whereby their effects remain unnoticed in the final measurement of the equalised system. Another application that requires highly accurate linear transfer function measurement is a technique proposed by the Authors to measure low level errors within audio systems [2].

There are three basic methods of transfer function measurement; periodic impulse excitation (PIE), maximum length sequences (MLS) and time delay spectrometry (TDS). PIE reveals the periodic impulse response (PIR) of the device under test (DUT) directly by applying a periodic short duration impulse to the DUT and averaging the output over several measurement periods [3]. The main problem encountered in PIE is poor noise immunity due to low excitation signal power; this drawback is overcome to a large degree by using MLS which, compared to periodic impulses of similar repetition rate, have a much higher excitation power for the same peak output (i.e a lower crest factor). MLS are essentially pseudo-random binary sequences which yield a unit impulse upon circular auto-correlation. This property allows the PIR of a test system to be obtained by applying an MLS to the DUT and cross-correlating the system output with the input. An excellent introduction to MLS techniques is due to Rife and Vanderkooy [4]. Whereas PIE and MLS initially reveal the transfer function in the time domain, TDS yields transfer function information as a complex frequency response (which can of course be converted to the time domain by using the inverse Fourier transform). TDS techniques utilise swept sine waves which are input to the DUT and reveal the complex frequency response at the system output after hardware and/or software processing [5].

MLS DISTORTION IMMUNITY

TDS is similar in many ways to MLS in the way that noise and distortion immunity is increased over simple PIE techniques, even though the measurements are performed in different 'domains'. However, it can be shown that in achieving a similar frequency resolution to an MLS measurement, TDS will typically take considerably longer to execute unless a complicated postprocessing operation is performed [4],[5],[6]. The additional disadvantage that TDS suffers in terms of hardware and software complexity [7] also helps to explain the growing popularity of MLS [8],[9].

Noise and distortion present in any practical measurement system reduces the accuracy of transfer function determination. For example Figure 1 shows an fft of an MLS-derived impulse response simulation of a 1 kHz lowpass FIR filter with less than 0.001 dB passband ripple. The excitation has been distorted by a second order non-linearity at a peak level of 20 dB below the driving signal which causes the transfer function to appear much more ragged over the filter's passband than its linear specification would suggest.

This paper concentrates upon a comparison of the noise and distortion immunity of PIE and MLS techniques. After basic behaviour has been established, MLS distortion behaviour is more closely examined leading to some general conclusions concerning MLS applications.

1 COMPUTER SIMULATED COMPARISON OF PIE AND MLS NOISE AND DISTORTION IMMUNITY

Any system with a weak non-linearity can be modelled as a linear filter h(n) representing the linear transfer function and a non-linearity described by a distortion polynomial d{x}, possibly followed by a further filter haa(n) (see Figure 2). When the system is excited by either a PIE or an MLS then the impulse response ho(n) obtained after post-measurement processing will in general contain the linear component h(n) plus a non-linear component hd(n) due to d{x}:

$$ho(n) = h(n) + hd(n) \qquad (1)$$

In order to calculate the nature and magnitude of hd(n) we can calculate ho(n) with a certain d{x} and subtract from this h(n) (which is estimated by setting d{x} to zero). The following simulations generate such information by convolving the periodic driving signal (either a PIE or an MLS) with a known system impulse response h(n). If h(n) is non-zero for a time less than the period of the driving signal then time aliasing is avoided and just one period is required in the simulations to accurately describe the periodic system behaviour.

The convolved driving signal is distorted by polynomial d{x} and after appropriate post-processing has been performed to extract the distorted DUT impulse response ho(n), the error component hd(n) can be calculated by subtracting the known h(n) from ho(n). Note that haa(n) in Figure 2 models the anti-aliasing filter found in the ADC of a physical measurement system, with a cutoff frequency close to half the system sampling frequency. Its presence only marginally effects the results obtained below, hence it has been omitted from the simulations for clarity.

The generalised simulation process can be summarised thus:

$$\begin{aligned} Di(n) &= D(n) \otimes h(n) \\ Do(n) &= [1 + d[Di(n)]]\ Di(n) \\ ho(n) &= ID[Do(n)] \\ hd(n) &= ho(n) - h(n) \end{aligned} \qquad (2)$$

where D(n) is the raw driving signal applied to the system (i.e. either PIE or MLS of period L and unit amplitude);

$\otimes$ represents convolution;

Di(n) is the filtered driving signal input to the non-linearity model d{x};

Do(n) is the distorted driving signal;

ID[x] represents the post-processing operation required to yield an impulse response from the driving signal.

Unless otherwise specified, d{x} is calibrated at -20 dB relative to the peak value of the driving signal. For example a third order non-linearity could be written:

$$Do(n) = \left[1 + \frac{1}{10}\left(\frac{Di(n)}{|\,Di(n)\,|_{max}}\right)^3\right] Di(n) \qquad (3)$$

A more detailed description of the simulation process for both PIE and MLS will now follow.

1.1 PIE Distortion Immunity

Periodic impulse testing reveals the periodic impulse response of the DUT directly; no post-processing is required since the driving signal is itself an impulse, though averaging several impulse periods can improve random noise immunity (see section 1.1.1). Hence ID[x(n)] = x(n), and the PIE simulation process can be summarised as:

$$\begin{aligned} Di(n) &= h(n) \\ ho(n) &= Do(n) = [1 + d[h(n)]]\ h(n) \end{aligned} \qquad (4)$$

In the following simulations the raw driving signal D(n) is a unit impulse with a period L of 2048 samples. This signal is convolved with a system impulse response h(n) formed by a 20 kHz lowpass FIR filter and representing, say, a DAC reconstruction filter driving a system with a perfectly flat frequency response. The specifications of this and other lowpass FIR filters used in the simulations are listed in Table I. h(n) is illustrated in the frequency domain in Figure 3 (for this and other

examples the fft results have been scaled so that an unfiltered periodic unit impulse has an amplitude of 0 dB across the spectrum; further note that all ffts are unwindowed since they transform *periodic* signals).

Table I Specifications for FIR filters used in the simulations (44.1 kHz sampling frequency).

Filter Type	Passband Cutoff Frequency kHz	Stopband Cutoff Frequency kHz	Passband Ripple dB	Stopband Attenuation dB	Group Delay Samples
Lowpass	1	2	0.0001	100	143
Lowpass	20	21	0.0001	100	143
Bandpass	14,18	13,19	0.006	63	86

PIE distortion immunity is now examined by distorting the filtered driving signal with a 2nd order non-linearity of relative level -20 dB. The distorted component hd(n) of the impulse response distortion is plotted in isolation in Figure 4a, and can be seen to be smoothly distributed in the frequency domain. This occurs because PIE errors due to non-linearities will generally be concentrated around the linear impulse in the time domain and hence will be impulse-like in nature (Figure 4b). Figure 4c shows the same measurement as Figure 4a but this time with the driving signal distorted by a 3rd order non-linearity. The distortion is distributed in the frequency domain in a similar fashion to that of the 2nd order distortion but at a slightly lower level; this discrepancy is accounted for by the difference between 2nd and 3rd order distortion characteristics and the peak calibration of distortion levels.

PIE noise immunity is simulated by adding to the driving signal a noise signal with an amplitude probability density distribution (pdf) shown in Figure 4d, indicating near Gaussian characteristics. This signal is scaled such that it has an rms value 60 dB below the peak value of the driving signal to which it is then added. Subtracting the corrupted impulse response from the linear response will of course simply reveal the attenuated noise signal (Figure 4e) indicating flat frequency response.

1.1.1 Optimum PIE Excitation Level

We have seen that distortion immunity of PIE-derived measurements is approximately equal to the relative peak level of the distortion for low order non-linearities. Noise immunity is equal to the rms level of the system noise below the rms level of the driving signal, i.e. no additional noise rejection is offered by PIE measurements. The total error level in a PIE measurement will equal the sum of distortion error and noise error, and it is obviously desirable to minimise this total error by careful choice of driving signal amplitude. Generally, if the driving signal amplitude is increased then for a fixed system distortion and noise characteristic the proportion of total error due to distortion will increase and that due to noise will decrease. The opposite will occur when the driving signal amplitude is decreased. Therefore the optimum driving signal level occurs when the total error contributions from noise and distortion are equal. With some knowledge of the noise and distortion performance of the system under test it is possible to make a fairly accurate estimation of the optimum driving signal amplitude that will result in minimum total error. Averaging the results of N measurements will reduce the noise contribution by a factor of $\sqrt{N}$ while the deterministic error due to distortion will remain constant. Thus averaging also reduces the optimum driving signal amplitude.

1.2 MLS Distortion Immunity

In the following simulations the driving signal is a binary maximum length sequence s(n) of period L = 2047 samples and unit amplitude; this is generated in software by an 11-stage shift register with an appropriate exclusive-OR feedback structure [10]. The driving signal is then convolved with the linear impulse response of the simulated system, again a 20 kHz lowpass FIR filter. The convolution is most efficiently performed in the frequency domain over 4096 samples to avoid periodic time aliasing (see chapter 12 of [11]). Distorting the convolved driving signal will corrupt the impulse response obtained from the measurement but the nature of the distortion will be different from that of the PIE derived measurement since MLS techniques involve a post-processing operation, crosscorrelating the input driving sequence s(n) with the system output [4]. Hence

$$\begin{aligned} ID[x(n)] &= s(n) \;\Phi\; x(n) \\ &= \frac{1}{L+1} \sum_{k=0}^{L-1} s(k)\; x(n+k) \end{aligned} \tag{5}$$

Here Φ corresponds to a *circular* crosscorrelation operation across the measurement period L, hereafter referred to simply as a crosscorrelation. If s(n) is of unit peak amplitude then the crosscorrelation simply consists of additions and subtractions and can be efficiently performed by fast Hadamard transform [10],[12]. Now crosscorrelation is an associative process hence impulse distortion hd(n) can be calculated by crosscorrelating s(n) with the driving sequence distortion Dd(n). The MLS simulation summary is thus:

$$\begin{aligned} Di(n) &= s(n) \otimes h(n) \\ Do(n) &= [1 + d\{Di(n)\}]\; Di(n) \\ Dd(n) &= Do(n) - Di(n) \\ ho(n) &= s(n) \;\Phi\; Do(n) \\ hd(n) &= s(n) \;\Phi\; Dd(n) \end{aligned} \tag{6}$$

This procedure is followed to obtain Figure 5a which shows a 2048 point fft of the impulse distortion caused by a 2nd order non-linearity calibrated at 20 dB below the peak amplitude of the filtered driving signal Di(n) (in this and the following ffts of MLS signals the last point is extrapolated without significantly effecting the accuracy of the plots). This measurement is repeated in Figure 5b for 3rd order distortion. By comparing Figures 5a and 5b to 4a and 4c respectively, it is clear that the MLS-derived un-truncated impulse measurements offer an increase in distortion immunity of between 10 and 15 dB over equivalent PIE measurements. Figure 5c indicates the random signal immunity of the MLS measurement using the noise signal shown in Figure 4d calibrated at -60 dB with respect to the peak MLS amplitude. Note how the MLS noise immunity is approximately 33 dB greater than for the corresponding PIE case (Figure 4e). This agrees with the general result that MLS methods achieve a Gaussian noise immunity of $\sqrt{L}$, where L is the period of the MLS.

MLS DISTORTION IMMUNITY

For explanation of these results on an intuitive level, the error level due to additive Gaussian noise is reduced for the MLS measurement because random noise is uncorrelated to s(n) and hence hd(n) will tend to sum to zero from sample to sample during the crosscorrelation operation of Equation (6). However, this is not the case for non-linearities where distortion will to a degree be correlated with the unfiltered driving signal s(n), hence distortion immunity does not show the same improvement in moving from a PIE based measurement regime to an MLS one. This argument is given further weight by the slight improvement in MLS-based distortion immunity shown by 2nd order non-linearity (Figure 6a) compared to 3rd order (Figure 6b) since 2nd order distortion will be less correlated with the driving sequence than will 3rd. This is because even order driving distortion D2(n) will be of the same sign from sample to sample irrespective of the sign of the driving MLS while odd order errors are always related to the sign of the driving signal.

An alternative way of examining the differences between the two measurement strategies is to compare the various power levels in each system. For the same peak driving signal amplitude, the MLS driving signal has L times the energy that the periodic impulse based excitation does. Hence for an additive random noise signal of fixed amplitude, the signal to noise ratio increases by $\sqrt{L}$. However, distortion energy generally increases with driving signal energy, hence in changing from a PIE to an MLS measurement the distortion energy also increases and signal to distortion ratio does not change by a great deal.

1.2.1 Optimum MLS Excitation Level

For the same peak distortion amplitude, MLS excitation offers a 10 to 15 dB increase in distortion immunity over PIE for low-order non-linearity and an $\sqrt{L}$ increase in noise immunity, where L is the measurement period. Hence for the same error conditions and peak driving signal amplitude, MLS offers a minimum reduction in total error of 10 to 15 dB over PIE. However, like their PIE counterparts, MLS-based transfer function measurements possess minimum total error when the noise and distortion error contributions are of equal magnitude, and with an optimally chosen excitation amplitude the total error advantage can be up to $\sqrt{L}$. Because MLS noise immunity is higher than distortion immunity then an optimally set up PIE measurement is likely to have a higher peak amplitude than an optimal MLS arrangement measuring the same system. Like PIE measurements, MLS noise immunity is further increased by averaging several measurements, although again distortion errors remain unaffected. Thus optimum MLS excitation amplitude also decreases as averaging is effected.

2 NOISE AND DISTORTION IMMUNITY OF TRUNCATED MLS-DERIVED IMPULSE MEASUREMENTS

The noise and distortion immunity of MLS-derived impulse responses can be increased by truncating the impulse response achieved after cross-correlation. This is because the linear impulse response h(n) will typically be contained in the first few samples of the measurement while noise and distortion hd(n) will tend to be spread over the measurement period. Rife and Vanderkooy [4] suggest that non-linear MLS errors can be viewed as a phase-randomised signal in the frequency domain which should result in a time domain signal evenly spread over the measurement period. If the error energy is evenly spread then truncating the distorted impulse response of period L at t samples will result in an increase in signal to distortion ratio (SDR) of T dB given by:

MLS DISTORTION IMMUNITY

$$T = 10 \log_{10} \left[\frac{L}{t} \right] \tag{7}$$

To investigate the accuracy of this conjecture some tests were performed upon the impulse distortion hd(n) obtained from the above MLS simulations. Figures 6a and b indicate the distortion in the time domain for the 2nd and 3rd order non-linearity models respectively; the distortion appears to be anything but evenly spread across the measurement period. To examine how uneven the distributions are, a plot of distortion energy distribution Ed(n) for each of the simulations is presented in Figures 6c and d. Ed(n) is obtained by calculating error energy accumulation across the sequence as a proportion of total error energy:

$$Ed(n) = \frac{\sum_{k=0}^{n} hd(k)^2}{\sum_{k=0}^{L-1} hd(k)^2} \tag{8}$$

Hence for a perfectly smooth and even distribution Ed(n) should plot as a straight line from (sample 0, 0%) to (sample L, 100%). The distribution for the 2nd order non-linearity shown in Figure 6c shows about 40% of the total error energy concentrated around the linear impulse response (at approximately 140 samples into the measurement period), although the remaining error power is fairly evenly distributed. Hence if hd(n) were truncated at 256 samples to just include the linear part of the impulse response then the increase in SDR would only be 4 dB rather than the 9 dB expected from Equation (7). The 3rd order distortion distribution is shown in Figure 6d and indicates an even more severe error concentration around the linear impulse position. Such a distribution would present an SDR increase of only 0.2 dB if truncated at 256 samples and is a far cry from Rife and Vanderkooy's evenly distributed distortion model.

Why is there such a discrepancy between the even distortion distribution model and these results? Rife and Vanderkooy speculate that for the distortion to be evenly distributed the MLS stimulus should be quasi-Gaussian in order for non-linearities to be exercised over a wide range of levels. Figure 7 shows the pdf of the MLS driving signal Di(n) used in the simulations of Figures 5 and 6, where the raw binary signal has been lowpass filtered with a 20 kHz FIR filter. The amplitude probability distribution of this signal is evidently *not* Gaussian. In an attempt to make the stimulus more Gaussian the simulations were repeated using a 1 kHz lowpass FIR filter, resulting in the near-Gaussian MLS stimulus pdf shown in Figure 8a. The corresponding distortion distributions for 2nd and 3rd order non-linearities are indicated in Figures 8b and 8c respectively. The 1 kHz and 20 kHz filtered distributions are surprisingly similar for the 2nd order non-linearities but for the 3rd order distortions the 1 kHz filtered MLS-derived error is clearly better distributed with only 65% of error power distributed at the linear impulse position (representing a 1.9 dB improvement in SDR if truncated at 256 samples).

Another simulation example is shown in Figure 9, this time using an MLS period length L of 16383 samples. This example uses a measured loudspeaker impulse response (Celestion SL700) with a fairly flat frequency response to filter the raw MLS stimulus. Since the loudspeaker transfer function has many poles and zeroes then the pdf of the filtered MLS driving signal shown in Figure 9a is very nearly Gaussian. The corresponding error distribution for 2nd order distortion plotted in Figure 9b is

more or less even indicating an 8.2 dB improvement in SDR for truncation at 2048 (L/8) samples. However, Figure 9c shows that even for Guassian stimulus the 3rd order distortion distribution is far from even with 75% of error energy concentrated in the first 2048 samples.

A final example used to illustrate the efficacy of truncation schemes is similar to the example used by Rife and Vanderkooy in their attempt to justify the even distortion distribution model. Here h(n) is a bandpass filter of passband 14 to 18 kHz, specified in Table I and illustrated in the frequency domain with linear frequency scale in Figure 10. Two MLS of length 1023 and 16383 samples are filtered with h(n) yielding the pdf plots of Figures 11a and 12a respectively, indicating pseudo-Gaussian behaviour. These MLS driving signals are then distorted with 2nd and 3rd order non-linearities at -12 dB with respect to peak driving levels. The corrupted frequency responses extracted from the distorted MLS signals are shown in Figures 11b, 11c, 12b and 12c. Note how the distortion error appears to be similar in both nature and magnitude for both measurement lengths. Plots of distortion distribution for 2nd and 3rd order non-linearities are shown for L = 16383 in Figures 12d and 12e; truncating at 1024 samples should yield SDR increases for the longer length sequence of 10 and 1.5 dB for 2nd and 3rd order errors respectively. However, when the truncated impulse responses are plotted in the frequency domain they indicate a larger than expected increase in SDR over the 1023 point MLS plots for 3rd order non-linearity (compare Figure 12g to 11c). This contradiction is solved when the error is plotted in isolation (Figures 11d, 11e, 12h, 12i), showing that most of the error due to the 3rd order non-linearity is of fundamental nature and hidden in the earlier plots. A comparison of the 3rd order error curves (Figures 11e, 12i) also indicate the modest increase in SDR for the truncated 16383 point sequence predicted from the distortion distribution curves, certainly smaller than the figure of 12 dB predicted from the even distribution model.

Table II Increase in SDR for truncated MLS-derived impulse responses.

L	MLS Driving Filter	Distortion Order	Truncation Length t	Increase T in SDR due to Truncation dB
Even Distribution Distortion Model			L/8	9.0
2047	20 kHz Lowpass	2	256	4.0
2047	20 kHz Lowpass	3	256	0.2
2047	1 kHz Lowpass	2	256	3.7
2047	1 kHz Lowpass	3	256	1.9
16383	Loudspeaker	2	2048	8.2
16383	Loudspeaker	3	2048	1.2
Even Distribution Distortion Model			L/16	12
16383	Bandpass 14-18 kHz	2	1024	10
16383	Bandpass 14-18 kHz	3	1024	1.5

These results are summarised in Table II and suggest that for many non-Gaussian MLS stimulus the impulse error power due to non-linearities is *not* evenly distributed across the measurement period.

Further simulations have suggested that the 2nd order results are representative of all even order distortions. Similarly the 3rd order results are representative of odd order errors, and are generally different from those of the even order simulations. Even order errors tend to be more evenly distributed than those of odd order which are concentrated in the time domain around the region occupied by the linear portion of the impulse response. As the MLS stimulus becomes more Gaussian the even order distributions become more evenly spread over the measurement period. Odd order errors also spread out but show a marked reluctance to a completely even behaviour; the Authors have yet to experience a 3rd order error distribution where less than 50 % of total error power is concentrated adjacent to the linear impulse.

Thus truncating MLS-derived impulse responses will result in an increase in signal to distortion ratio but not generally by the amount indicated by the even distribution model (Equation (7)). This increase in distortion immunity is not achievable by truncating a PIE-derived impulse response since in this case *all* distortion is co-incident with the linear impulse (Figure 4b). However, it should be noted that although MLS-derived impulse measurements show a $\sqrt{L}$ increase in random noise immunity over PIE techniques, truncation does not result in a further increase in MLS noise immunity advantage. This is because additive noise is spread evenly over the measurement period for both techniques and hence truncating either an MLS-derived or a PIE-derived measurement will result in a similar increase in SNR.

3 CONCLUSIONS

A simulated comparison of PIE and MLS impulse measurement techniques has shown that MLS methods possess superior noise and distortion immunity. MLS distortion immunity advantage was identified at between 10 and 15 dB for low order non-linearities while the noise immunity advantage over PIE is approximately equal to $\sqrt{L}$ where L is the length of the measurement period. In order to take advantage of the high noise rejection inherent to MLS, optimum excitation amplitude may be lower than in an equivalent PIE measurement.

MLS distortion immunity can be further increased by truncating the measured impulse response after the linear component of the measurement has decayed to zero. However the increase in distortion rejection due to truncation will not in general be as large as that predicted from the even distortion distribution model proposed by Rife and Vanderkooy, because non-linear error energy tends to be unevenly distributed across the measurement period. The simulations presented indicate that 2nd order error components become more evenly spread as MLS excitation tends to a Gaussian amplitude distribution. Conversely 3rd order errors show a reluctance to conform to an even distribution even for Gaussian excitation, accumulating in the vicinity of the linear component of the impulse response and resulting in ineffective truncation. This behaviour is inherent to odd order errors because of a high correlation between MLS excitation and distortion.

4 REFERENCES

[1] R.G.Greenfield and M.O.J.Hawksford, "Efficient Filter Design for Loudspeaker Equalisation," presented 86th. Convention Audio Eng.Soc., preprint 2764, March 1989.

[2] C.Dunn and M.O.J.Hawksford, "Towards a Definitive Analysis of Audio System Errors," presented 91st Audio Eng.Soc Convention, October 1991.

[3] J.M.Berman and L.R.Fincham, "The Application of Digital Techniques to the Measurement of Loudspeakers," J.Audio Eng.Soc., Vol.25, No.6, June 1977.

[4] D.Rife and J.Vanderkooy, "Transfer-Function Measurement with Maximum-Length Sequences," J.Audio Eng.Soc., Vol.37, No.6, June 1989.

[5] J.Vanderkooy, "Another Approach to Time Delay Spectrometry," J.Audio Eng.Soc., Vol.34, No.7/8, July/August 1986.

[6] H.Beiring and O.Z.Pederson, "Comments on "Another Approach to Time-Delay Spectrometry"," J.Audio Eng.Soc., Vol.35, No.3, March 1987.

[7] R.Greiner, J.Wania and G.Nocjovich, "A Digital Approach to Time-Delay Spectrometry," J.Audio Eng.Soc, Vol.37, No.7/8, July/August 1989.

[8] J.Atkinson, "Measuring with MELISSA," Stereophile, February 1990.

[9] M.Colloms, Loudspeaker Reviews, Hi-Fi News and Record Review, December 1990.

[10] J.Borish, "Self-Contained Crosscorrelation Program for Maximum-Length Sequences," J.Audio Eng.Soc., Vol.33, No.11, November 1985.

[11] W.H.Press, B.P.Flannery, S.A.Teukolsky and W.T.Vetterling, "Numerical Recipes in C," Cambridge, 1988.

[12] J.Borish, "An Efficient Algorithm for Measuring the Impulse Response Using Pseudorandom Noise," J.Audio Eng.Soc, Vol.31, No.7, July/August 1983.

MLS DISTORTION IMMUNITY

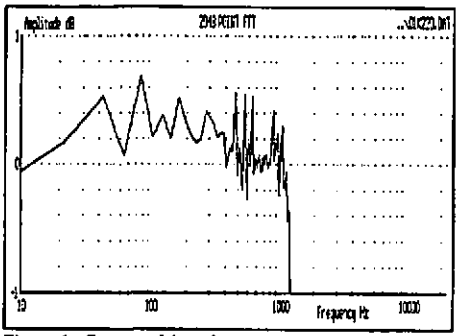

Figure 1 Corrupted impulse response measurement of 1 kHz lowpass filter with 2nd order distortion at -20dB.

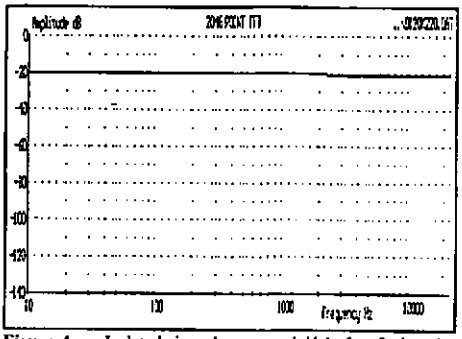

Figure 4a Isolated impulse error hd(n) for 2nd order distortion.

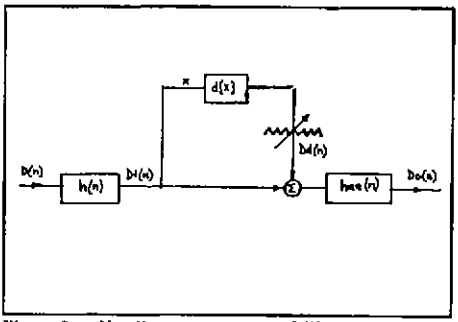

Figure 2 Non-linear system modelling for impulse response measurement.

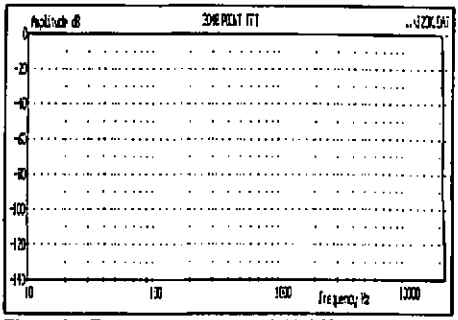

Figure 3 Frequency response of 20 kHz lowpass FIR filter.

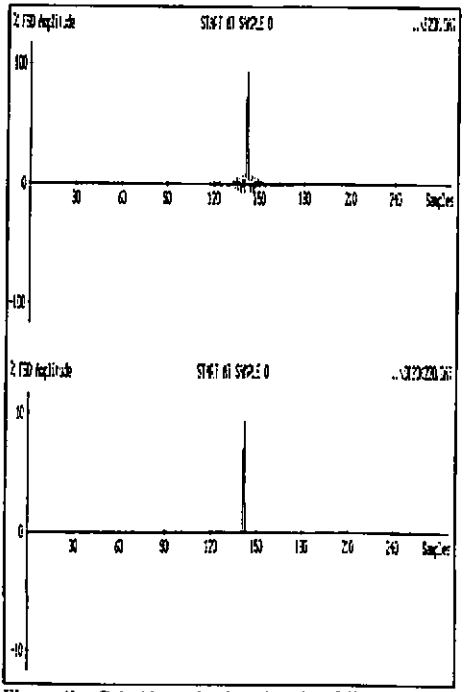

Figure 4b Coincidence in time domain of linear impulse response (top) and distortion error (bottom) for PIE measurement.

MLS DISTORTION IMMUNITY

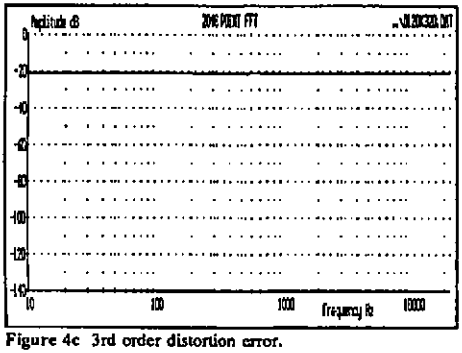

Figure 4c 3rd order distortion error.

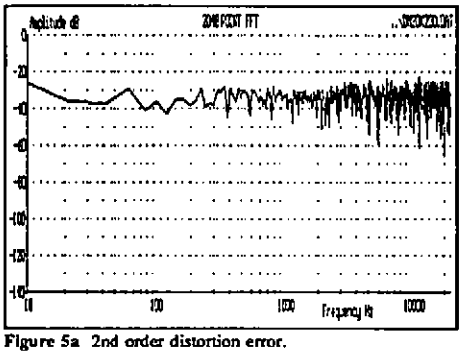

Figure 5a 2nd order distortion error.

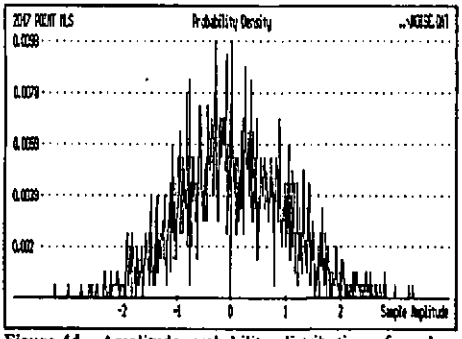

Figure 4d Amplitude probability distribution of random sequence used in noise immunity simulations.

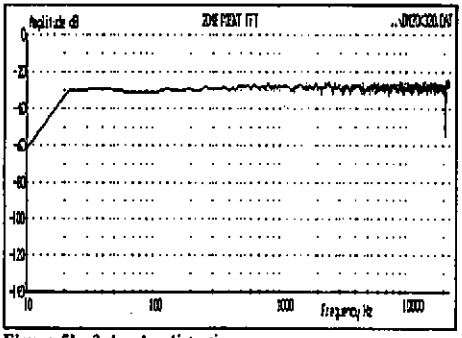

Figure 5b 3rd order distortion error.

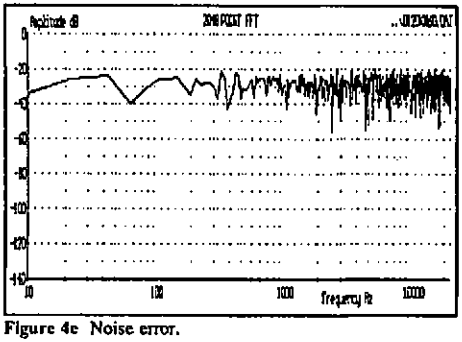

Figure 4e Noise error.

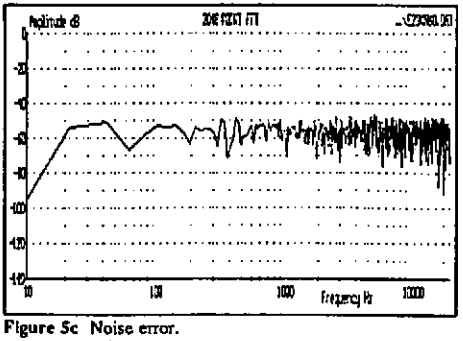

Figure 5c Noise error.

Figure 4 PIE error simulations for h(n) = 20 kHz lowpass filter.

Figure 5 MLS error simulations for h(n) = 20 kHz lowpass filter.

MLS DISTORTION IMMUNITY

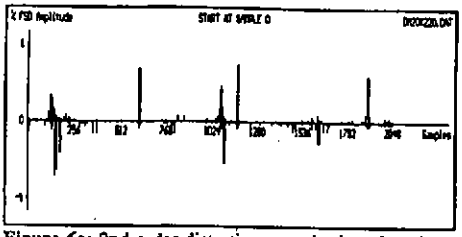

Figure 6a: 2nd order distortion error in time domain.

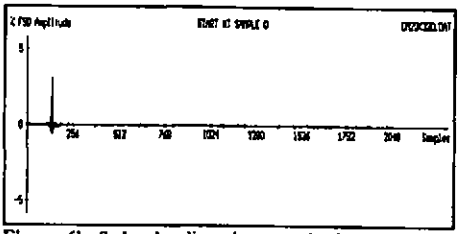

Figure 6b: 3rd order distortion error in time domain.

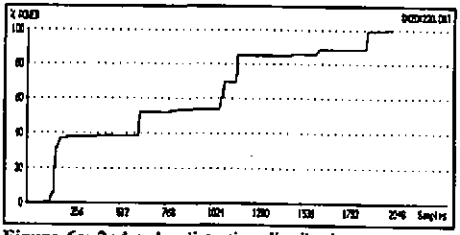

Figure 6c: 2nd order distortion distribution.

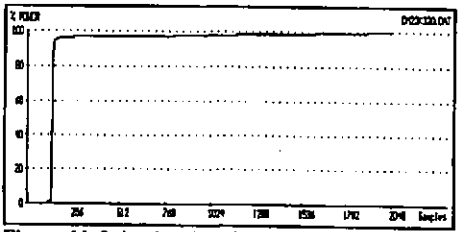

Figure 6d: 3rd order distortion distribution.

Figure 6: MLS distortion distributions for 20 kHz lowpass simulations.

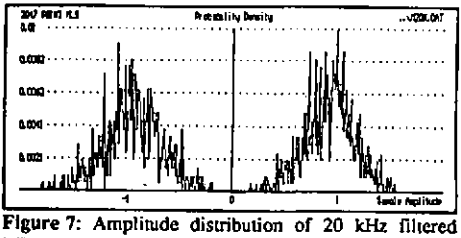

Figure 7: Amplitude distribution of 20 kHz filtered MLS.

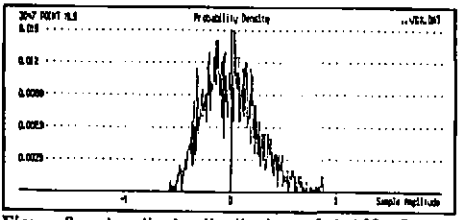

Figure 8a: Amplitude disribution of 1 kHz filtered MLS, indicating more Gaussian-like behaviour compared to Figure 7.

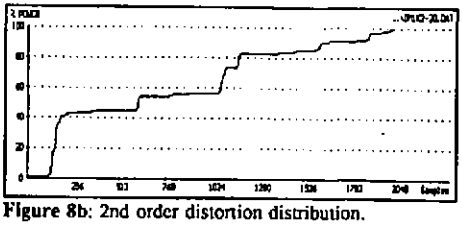

Figure 8b: 2nd order distortion distribution.

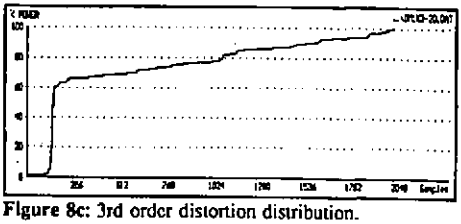

Figure 8c: 3rd order distortion distribution.

Figure 8: MLS errors for 1 kHz lowpass simulations.

MLS DISTORTION IMMUNITY

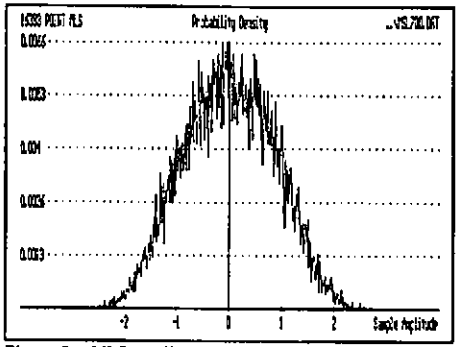

Figure 9a MLS amplitude pdf for loudspeaker simulation.

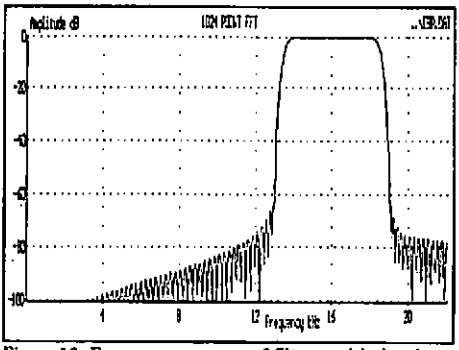

Figure 10 Frequency response of filter used in bandpass simulations.

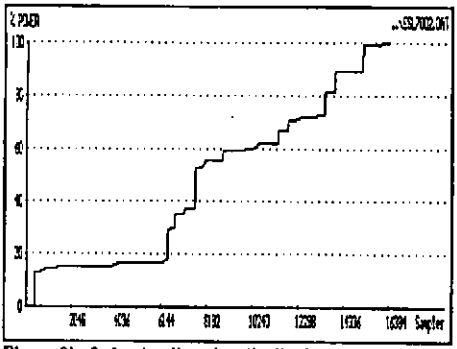

Figure 9b 2nd order distortion distribution.

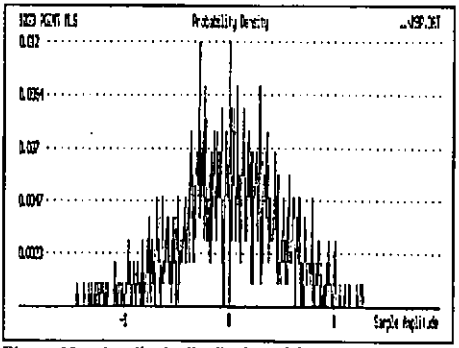

Figure 11a Amplitude distribution of filtered MLS.

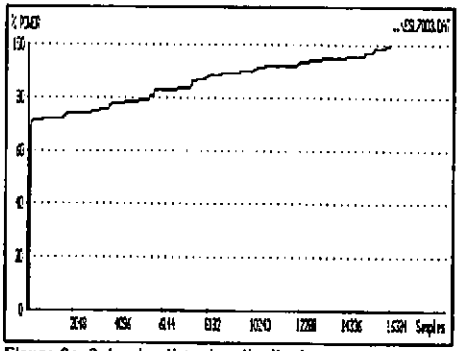

Figure 9c 3rd order distortion distribution.

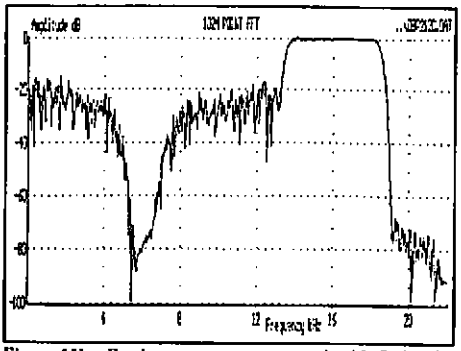

Figure 11b Bandpass response corrupted with 2nd order distortion.

Figure 9 MLS errors for loudspeaker simulations.

MLS DISTORTION IMMUNITY

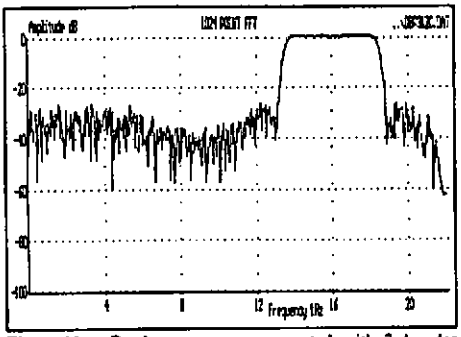

Figure 11c Bandpass response corrupted with 3rd order distortion.

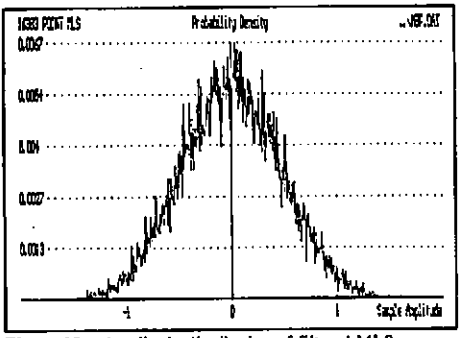

Figure 12a Amplitude distribution of filtered MLS.

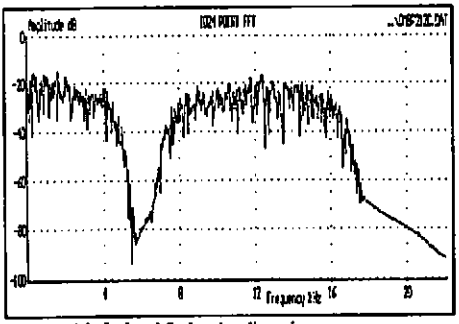

Figure 11d Isolated 2nd order distortion error.

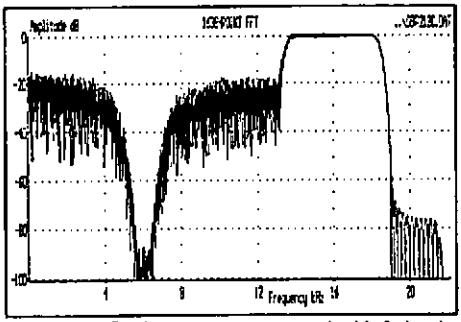

Figure 12b Bandpass response corrupted with 2nd order distortion.

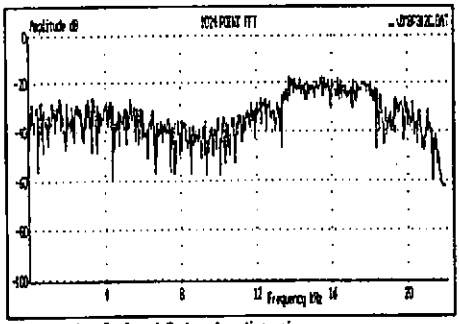

Figure 11e Isolated 3rd order distortion error.

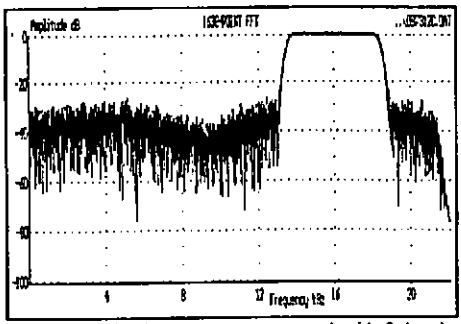

Figure 12c Bandpass response corrupted with 3rd order distortion.

Figure 11 Distortion error simulations of bandpass filtered 1023 point MLS.

MLS DISTORTION IMMUNITY

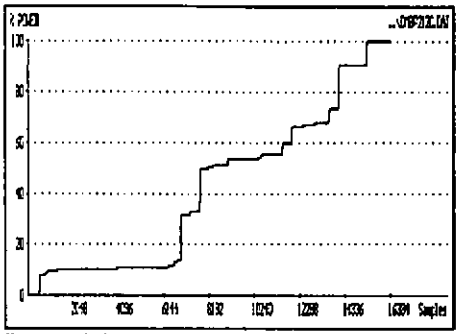

Figure 12d 2nd order error distribution.

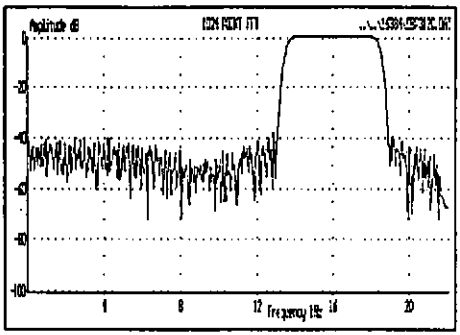

Figure 12g 3rd order corrupted impulse response truncated at 1024 samples.

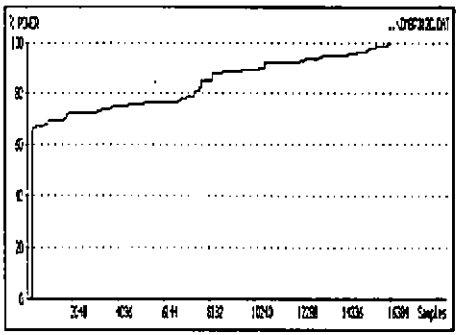

Figure 12e 3rd order error distribution.

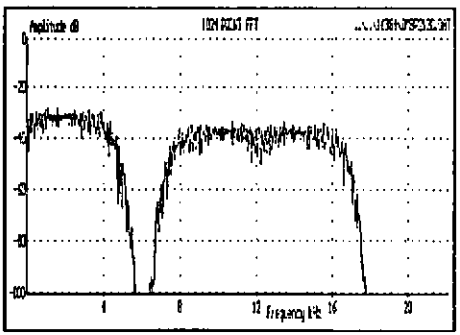

Figure 12h Isolated 2nd order error.

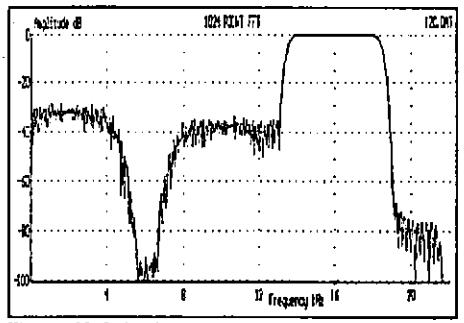

Figure 12f 2nd order corrupted impulse response truncated at 1024 samples.

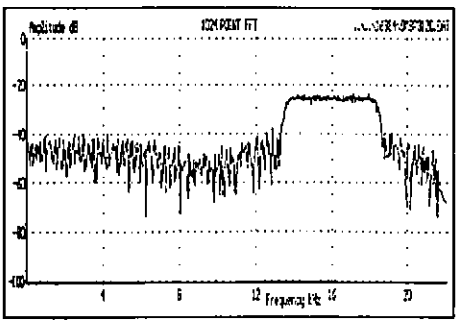

Figure 12i Isolated3rd order error.

Figure 12 Distortion error simulations of bandpass filtered 16383 point MLS.